Experiment on a Permanent Magnet-Biased Magnetic Bearing with a Cascade Digital Control

Mohamed S. Kandil *, Maxime R. Dubois *, Loicq S. Bakay †, João P. Trovão *

**e-TESC Laboratory, Department of Electrical & Computer Engineering, Université de Sherbrooke, Canada, ({Mohamed.Kandil; Maxime.Dubois; Joao.Trovao}@USherbrooke.ca)*
†GE Renewable Energy, Canada (loicqbakay@gmail.com)

Keywords: Magnetic Bearings, Digital Control, Energy Storage, Flywheels.

Abstract

A permanent magnet-biased active magnetic bearing (PM-AMB) is an efficient design of pure active magnetic bearing systems. This paper presents a digital decentralized double-loop controller for a radial homopolar PM-AMB. The inner loop is for current control while the outer loop is the master one and is devoted for regulation the shaft position around the operating point despite the harmonic excitation forces due to the inherent rotor unbalance. The Spectrum Digital eZdsp F2812 board is used for control implementation. Experimental results are given to validate the performance of the system followed by calculation of the power consumed by the radial bearing.

1 Introduction

An active magnetic bearing (AMB) is a mechatronic system that have been widely used to achieve a contactless support for a spinning rotor. It is an inherently nonlinear and an open-loop unstable system, thus a feedback control loop is a must to attain stability besides achieving a satisfactory performance. It is not surprising that most of the literature on AMBs concerns control schemes [1]. The commonly used control scheme for AMBs adopt a fixed bias current supplied to each coil to improve the linearity and dynamic performance, and to enable a single power amplifier per axis (less costly) if differential winding connection is adopted.

Another challenge connected to AMBs is their power consumption. Although the losses are much lower than roller bearings, these losses can limit the operation in some applications such as flywheel energy storage systems and vacuum applications [2]. Copper losses which is proportional to the square of the current flowing in the coils have a key role in the power losses in magnetic bearings. Other losses such as iron losses are also proportional to the coil current. Therefore enhancing the energy efficiency of magnetic bearings depends on minimizing coil currents.

There are two approaches to improve the energy efficiency of magnetic bearings [3]. For the first approach which adopts the software solution, various feedback control strategies which eliminate or reduce the fixed bias current have been proposed in order to minimize power losses [4], [5]. However besides the complexity of control schemes, lowering or eliminating the bias current could lead to poor dynamic performance and less robustness against disturbances so researchers studied a variable bias current strategy as in [2]. The hardware solution is an alternative approach which depends on employing permanent magnets [3], [6], [7]. In PM-AMBs, permanent magnets (PMs) provide the fixed bias flux while the control currents are used only for stabilization and damping vibrations. One of the first contributions to the design of PM-AMBs is reported in [8][9].

This paper discusses the digital implementation of a decentralized feedback control for a radial homopolar PM-AMBs using the cascade control structure. In the paper, the PID controller is used in the outer loop for position control while the PI controller is used for the inner loop to control the current. The continuous time controller is then discretized to obtain its digital counterpart. The Spectrum Digital eZdsp F2812 board is used for control implementation. The main contribution to this paper is the application of a radial homopolar PM-AMB to support a spinning shaft with a larger-scale size and heavier weight compared to the majority of reported cases in literature [3], [7]–[11] as well as the DSP implementation of the cascade controller. The description of the employed system as well as a simplified mathematical model are given first. The discretization process is then explained. Experimental results are given to validate the effectiveness of the closed loop system under different operating conditions.

2 System Description

The radial PM-AMB has two lamination stacks of four teeth each. In between the two lamination stacks are located the PM segments, as described in [6], see Fig. 1. Each tooth is wound with a coil of N turns (N = 100) and these 8 stator coils are positioned along the vertical (4 coils) and horizontal (4 coils) axes, thus forming 4 electromagnet (EM) poles. The four EM coils for each of the two axis are connected in series, thus 4N coils per axis. Fig. 2 shows a picture of the test rig. The driven terminal of the shaft is supported by a mechanical ball bearing while the non-driven terminal is supported by the radial homopolar PM-AMB. The rotation is realized through an induction motor which is connected to the shaft by means

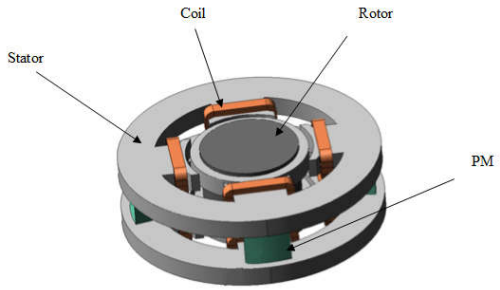

Fig. 1 Radial homopolar PM-AMB.

of a flexible coupling. Two single phase inverter circuits (one for each axis) are used to amplify the control current. The inverter is realized with a full H-bridge configuration consisting of four IGBTs with 30V DC-link because bidirectional current is needed for homopolar PM-AMB applications unlike pure AMBs which can employ half H-bridge configuration. Sensors are a must to close the feedback control loop. Two position sensors are used; one to monitor the deviation along the horizontal axis while the other one to monitor the deviation along the vertical axis. The position sensors are of inductive type. Their linear span is from 0 to 2 mm with a resolution of 1 μm. Most off the shelf current amplifiers of this type utilize an on-board analog PI control. In this work a digital current control is employed because of the flexibility in implementation and tuning compared to analog control. Hence two current sensors are also required for closing the current control loop.

2.1 The Rotor-Bearing System Model

The net electromagnetic force of a homopolar PM-AMB generated per axis can be formulated as [12]

$$F = \frac{A_g}{\mu_o}\left\{\left(B_{pm} + B_c\right)^2 - \left(B_{pm} - B_c\right)^2\right\} \qquad (1)$$

where A_g is the air-gap area under one tooth, μ_o is the permeability of free space, B_{pm} is the air-gap flux density due to PMs while B_c is the air-gap flux density due to control coils. It is common to linearize the force formula around the operating point and use the following simplified expression

$$F = k_s\, q + k_c\, i \qquad (2)$$

where k_s and k_c are the positon stiffness and force to current gain respectively, q is the position signal deviation measured from the equilibrium point, i is the control current .

It is assumed that the rotor is symmetric and rigid, and the axial motion is decoupled from the radial ones. Therefore the radial dynamics can be represented by 4 degrees of freedom (DOF) while the axial dynamics is 1-DOF which is not being of particular interest here. The equation of motion for a rotor suspended with a HMB and a ball bearing can be formulated as [13]

$$\mathbf{M}\ddot{\mathbf{p}} + \left(\omega\mathbf{G} + \mathbf{B}\mathbf{C}_{bb}\mathbf{B}^T\right)\dot{\mathbf{p}} + \left(\mathbf{B}\mathbf{K}_s\mathbf{B}^T + \mathbf{B}\mathbf{K}_{bb}\mathbf{B}^T\right)\mathbf{p} = \mathbf{B}\mathbf{K}_\mathbf{i}\mathbf{i} + \mathbf{F}_{un} \qquad (3)$$

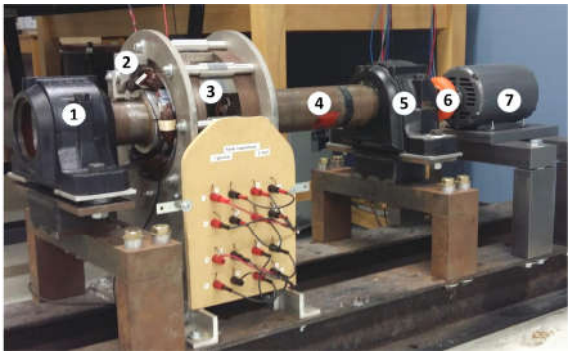

Fig. 2 Radial HMB test rig: (1) Safety bearing, (2) Position sensor, (3) HMB, (4) Shaft, (5) Ball bearing, (6) Flexible coupling, (7) Induction Motor

where

p	center of gravity coordinate
M	mass matrix
G	gyroscopic matrix
B	coordinate transformation matrix
$\mathbf{C}_{bb}$	damping matrix
$\mathbf{K}_s$	HMB stiffness matrix
$\mathbf{K}_{bb}$	ball bearing stiffness matrix
$\mathbf{K}_i$	force to current factor matrix
$\mathbf{F}_{un}$	harmonic vibration forces matrix
ω	rotation speed in rad/s

2.2 Electrical Dynamics

It is assumed that the total resistances and inductances of each of the two control windings are equal to R and L respectively. The electrical dynamics per axis in the system can be described as

$$\frac{di}{dt} = \frac{k_g}{L}v - \frac{R}{L}i \qquad (4)$$

where k_g is the current amplifier gain, v is the control voltage.

3 Digital Controller

A single radial magnetic bearing is usually represented as a two mechanical DOFs system for rigid body rotor, where each DOF describes the deviations of the shaft in the horizontal and vertical directions. The dynamics of the two directions can be decoupled if the gyroscopic effect is not significant which is true here. Thus two separate feedback control systems can be designed for each mechanical DOF, this is the so called decentralized control approach.

3.1 Cascade Control Structure

The commonly used control structure for both electric drives and magnetic bearings is the cascade-loop control “or double-loop control” [1][14]. The inner control loop is responsible for controlling the current. For AMBs, the outer control loop is the primary or the master loop and is devoted for

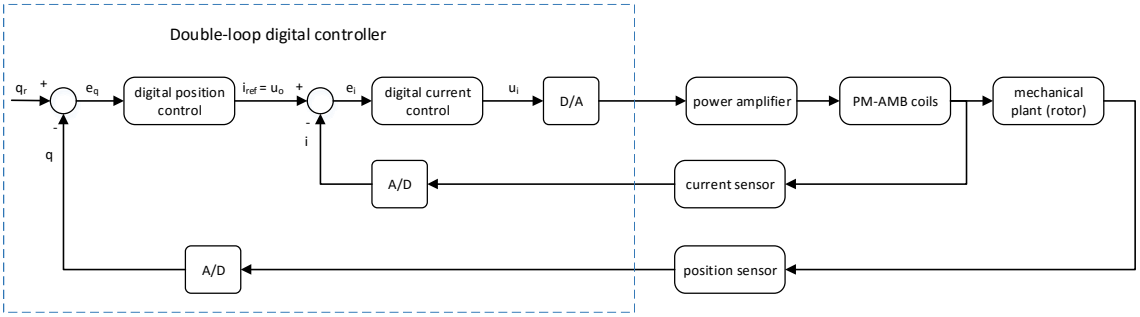

Fig. 3 Digital double-loop control structure

controlling the shaft position. The primary objective of the feedback control system is to stabilize the inherently unstable system first and then regulating the shaft position around the set-point. The input to the system is the position reference signal (usually the geometric center position of the bearing), and the output signal is the position of the shaft. Fig. 3 illustrates the employed controller structure.

3.2 Inner Control Loop

The function of the inner loop is to regulate the measured current i to track the current reference signal i_{ref} generated by the outer control loop. The current error is amplified and used to calculate the corresponding duty cycle to control the output voltage of the H-bridge. By employing a high-gain controller, it is expected that the control current can follow accurately the current reference signal. It is unadvised to use a high proportional feedback gain (P-controller) only, because the current amplifier will be prone to saturation as well as the high tendency of noise generation. The typical approach is to use a proportional-integral (PI) for current control. The current error signal e_i can be described as

$$e_i = i_{ref} - i \tag{5}$$

The continuous-time PI controller for the inner loop in the so-called parallel form is formulated as

$$u_i(t) = c_p . e_i(t) + c_i . \int_0^t e_i(\tau)\, d\tau \tag{6}$$

where c_p is the proportional gain and c_i is the integral gain for the inner control loop. And the Laplace equivalent form is

$$U_i(s) = \left(c_p + \frac{c_i}{s} \right) E_i(s) \tag{7}$$

3.3 Outer Control Loop

The outer loop, which is also known as position control loop, is the main controller. Since AMBs are inherently open loop unstable systems, the first goal of the main controller is to stabilize the system to the equilibrium point. The intuitive reasoning is to imitate the mass-spring-damper (MSD) system. Hence the controller is required to provide a restoring force similar to the mechanical spring as well as a damping component to dampen oscillations around the equilibrium point [1]. The simplest controller to achieve these requirement is the well-known proportional-derivative (PD) controller. For practical application, with a PD control there is always an offset error between the controlled variable and the set-point, no matter how high the P-gain. Addition of integral action is the remedy to this situation since it is able to eliminate this offset error. Hence the outer control loop for real systems becomes the proportional-integral-derivative control (PID). The position error e_q between the position reference signal q_r and the measured position signal q can be defined as

$$e_q = q_r - q \tag{8}$$

The PID controller for the outer loop in Laplace domain can be described as

$$U_o(s) = \left(k_p + \frac{k_i}{s} + k_d\, s \right) E_q(s) \tag{9}$$

where k_p is the proportional gain, k_i is the integral gain, and k_d is the derivative gain for the outer control loop. The expression of the controller given in Equation (9) cannot be implemented in practice. First of all because the transfer function of the controller is not proper[1]. The other problem is that a pure derivative action is not allowable in practice because of the amplification of the high frequency measurement noise. The commonly used solution to these problems is to cascade the derivative term with a low pass filter. The practical form of PID controller can be written as

$$U_o(s) = \left(k_p + \frac{k_i}{s} + \frac{k_d\, s}{1 + \tau\, s} \right) E_q(s) \tag{10}$$

where τ is the time constant of the low pass filter.

3.4 Controller Discretization

The current controller and the position controller were described by Laplace transform in Equations (7) and (10) respectively. Since we want to implement these controllers in digital form, it is necessary to represent them in discrete-time. The commonly used approach for designing a digital

[1] In control theory, a transfer function is proper if its numerator does not exceed its denominator.

controller for a continuous-time system is to first design an analog controller and then convert it into an equivalent discrete-time system that have a close approximate behavior [15]. There are various techniques from the signal processing field that can be used to convert an analog controller to its digital form counterpart. The method we are going to use is the approximation of differential equations by numerical integration. There are commonly three methods for this purpose, Forward Euler (FE), Backward Euler (BE), and Trapezoidal method or Tustin's method. In this section we present the discretization of the position controller and the current controller can be done in a similar manner. Discretizing a continuous-time system by Tustin method can simply be done by replacing the Laplace variable s with

$$s \approx \frac{2}{T_s}\left(\frac{z-1}{z+1}\right) \tag{11}$$

where T_s is the sampling time and z is the variable of Z-transform. By following this rule, the integral and derivatives terms can be discretized respectively as follows

$$I(z) = \frac{k_i T_s}{2}\left(\frac{z+1}{z-1}\right) \tag{12}$$

and

$$D(z) = \frac{2k_d}{T_s + 2\tau} \cdot \frac{z-1}{z + \left(\frac{T_s - 2\tau}{T_s + 2\tau}\right)} \tag{13}$$

Since the proportional part is static, no discretization is needed and thus

$$P(z) = k_p \tag{14}$$

and the complete outer-loop control signal would be

$$U_o(z) = \{P(z) + I(z) + D(z)\} E(z) \tag{15}$$

4 Experimental Results

Table 1 presents the parameters of the system. Two decentralized feedback controllers are used to control the

Rotor mass (m)	61.9 kg
Rotor transverse moment of inertia	4.79 kg m^2
Rotor polar moment of inertia	0.086 kg m^2
Force to current factor ($k_{cx} = k_{cy}$)	609 N/A
HMB stiffness for horizontal motion (k_{sx})	28.05 N/mm
HMB stiffness for vertical motion (k_{sy})	47.8 N/mm
Nominal PM-AMB air-gap length	1 mm
Nominal safety bearing clearance length	0.5 mm
Coil resistance (R)	1.137 Ω
Coil inductance (L)	0.136 H
DC voltage supply	30 V

Table 1 MODEL DATA FOR ROTOR-BEARING SYSTEM

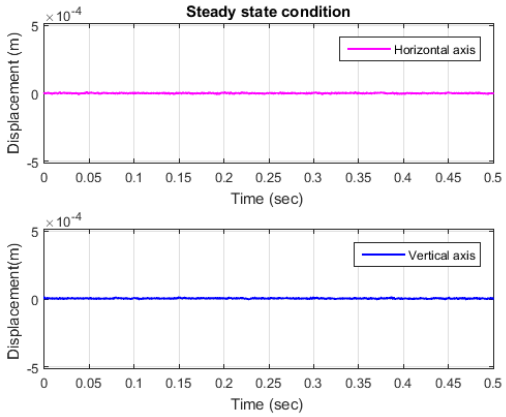

Fig. 4 Rotor horizontal and vertical displacements at 0 rpm

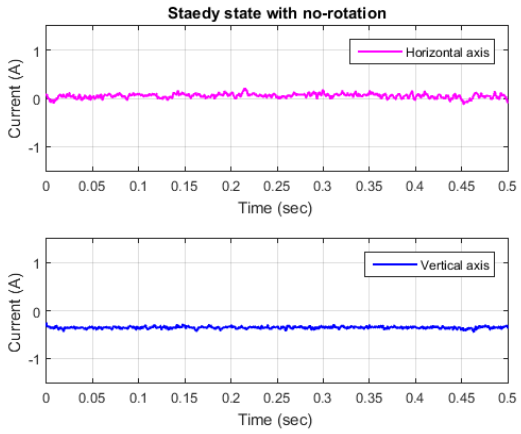

Fig. 5 Rotor horizontal and vertical currents at 0 rpm

radial hybrid magnetic bearing. The control parameters for the inner and outer loops were initially selected in simulation using the system model described by (3) built in Matlab/Simulink environment and then finely tuned after extensive experimentation to

$c_p = 3$, $c_i = 10$, $k_p = 3300$, $k_i = 20000$, $k_d = 8$, $\tau = 0.001$

The control algorithm is implemented using the Spectrum Digital eZdsp F2812 board. The board employs TMS320F2812 DSP which is a 32-bit DSP with fixed-point arithmetic and includes six dual PWM channels and 16 ADCs. Analog anti-alias low pass filters with 1.5 kHz cut-off frequency are used to attenuate the effect of high frequency measurement noise. A sampling rate of 10 kHz is used.

4.1 System Performance at 0 RPM

Fig. 4 shows the horizontal and vertical displacements of the levitated shaft at steady state with 0 rpm rotation speed. The peak-to-peak (P2P) displacement for the horizontal axis is 19.84 μm while for the vertical direction it is 7.92 μm. The corresponding control efforts for the non-rotation steady state condition are given in Fig. 5.

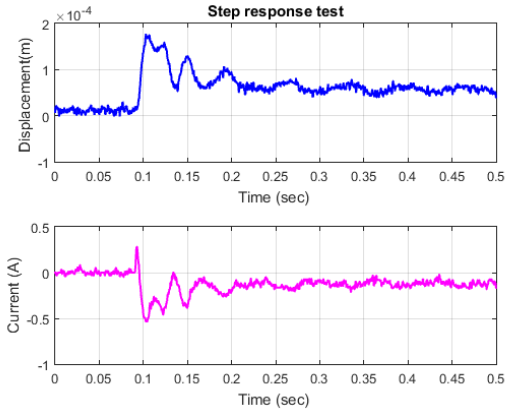

Fig. 6 Step response – horizontal direction

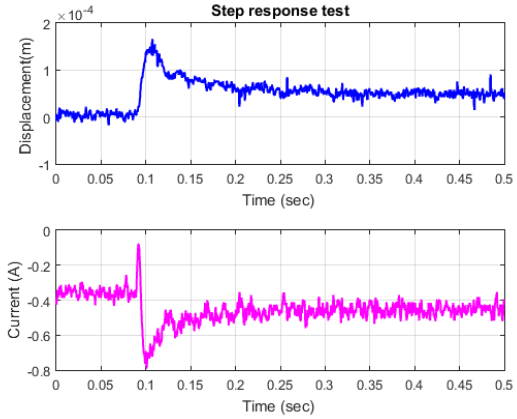

Fig. 7 Step response – vertical direction

4.2 Step Response

Fig. 6 shows the transient response for a 0.05 mm step applied to the input of the horizontal direction closed loop. The upper part of the figure illustrates the horizontal displacement while the corresponding control current is presented in the lower part. The step response for the vertical direction is presented in Fig. 7. The maximum horizontal displacement is 0.178 mm with 255% peak overshoot (PO) while the maximum vertical displacement is 0.166 mm with 232% PO. The time required for the vertical direction to settle within $\pm 5\%$ of the equilibrium position is 0.1158 seconds. For horizontal direction, it takes 0.1162 seconds to reduce oscillations to amplitudes of 30% of the steady state value before the system settles after approximately 0.41 seconds.

4.3 System Performance under Rotation

Two cases are given to address the behavior of the system during rotation. Fig. 8 shows the vibration level of the shaft spinning at 1000 rpm. The P2P horizontal displacement is 0.1325 mm while the P2P vertical vibration amplitude is 0.1058 mm. The control currents for the horizontal and vertical axes for the 1000 rpm case are illustrated in Fig. 9.

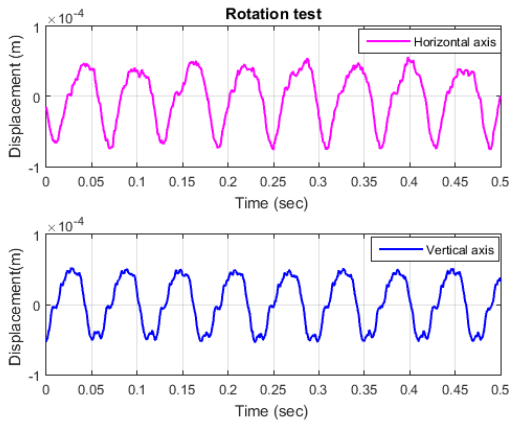

Fig. 8 Rotor horizontal and vertical displacements at 1000 rpm

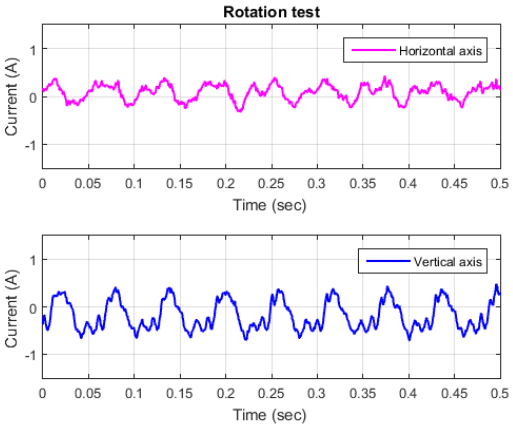

Fig. 9 Rotor horizontal and vertical currents at 1000 rpm

The second case is for the system rotating at 1800 rpm. The horizontal and vertical vibration amplitudes are shown in Fig. 10. The P2P horizontal and vertical displacements are 0.0877 mm and 0.113 mm respectively. The corresponding control efforts are shown in Fig. 11. The maximum vibration amplitude for both cases is approximately 0.068 mm which represents 13.6% of the 0.5 mm safety bearing clearance.

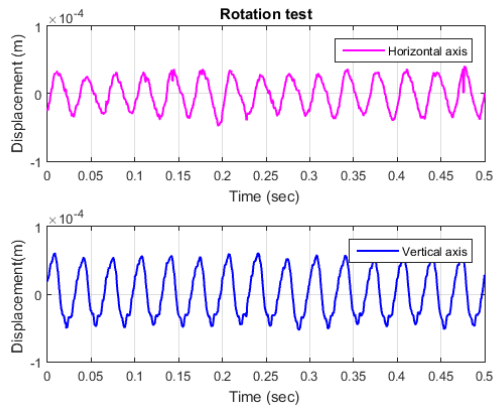

Fig. 10 Rotor horizontal and vertical displacements at 1800 rpm

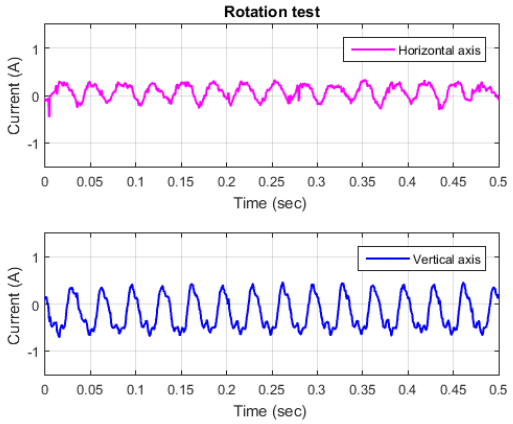

Fig. 11 Rotor horizontal and vertical currents at 1800 rpm

4.4 Power Loss Evaluation

The power consumption of the radial homopolar PM-AMB is evaluated for two operating conditions 1000 rpm, and 1800 rpm by calculating the ohmic loss according to

$$P_{loss} = I_x^{\,2} R_x + I_y^{\,2} R_y \qquad (16)$$

where I_x and I_y are the root-mean-square (RMS) value of the control currents flowing in the electromagnetic coil of the horizontal and vertical directions respectively. R_x and R_y represents the total resistance for the horizontal and vertical coils respectively. The total ohmic losses for the radial bearing are 0.182 watts and 0.205 watts for the first and second cases respectively.

5 Conclusion

This paper presents the digital implementation of a decentralized double-loop controller for a radial PM-AMB of the homopolar configuration. The description of the employed system as well as a simplified mathematical model are given first. The employed controller is then discussed. PI controller is used for the inner loop while PID control is used for the outer loop. Tustin method is used to discretize the feedback controller. Experimental results are given to validate the satisfactory performance of the closed loop system under different operating conditions. The maximum vibration amplitude for the studied cases is approximately 0.068 mm which represents 13.6% only of the 0.5 mm safety bearing clearance. The total ohmic losses consumed by one radial PM-AMB is approximately no more than 0.21 watts at 1800 RPM rotation speed.

References

[1] H. Bleuler, M. Cole, P. Keogh, R. Larsonneur, E. Maslen, Y. Okada, G. Schweitzer, A. Traxler, and E. H. Maslen, *Magnetic Bearings: Theory, Design, and Application to Rotating Machinery*. Berlin, Heidelberg: Springer Berlin Heidelberg, 2009.

[2] M. N. Sahinkaya and A. E. Hartavi, "Variable Bias Current in Magnetic Bearings for Energy Optimization," *IEEE Trans. Magn.*, vol. 43, no. 3, pp. 1052–1060, Mar. 2007.

[3] E. H. Maslen, P. E. Allaire, M. D. Noh, and C. K. Sortore, "Magnetic bearing design for reduced power consumption," *J. Tribol.*, vol. 118, no. 4, pp. 839–846, 1996.

[4] P. Tsiotras and B. Wilson, "Zero- and low-bias control designs for active magnetic bearings," *IEEE Trans. Control Syst. Technol.*, vol. 11, no. 6, pp. 889–904, Nov. 2003.

[5] S. Ueno and M. N. Sahinkaya, "Adaptive Bias Current Control in Active Magnetic Bearings for Energy Optimization," *Volume 1: 23rd Biennial Conference on Mechanical Vibration and Noise, Parts A and B*. 2011.

[6] L. Bakay, M. Dubois, P. Viarouge, and J. Ruel, "Losses in hybrid and active magnetic bearings applied to Long Term Flywheel Energy Storage," *Power Electronics, Machines and Drives (PEMD 2010), 5th IET International Conference on*. pp. 1–6, 2010.

[7] S. Cheng and S. W. Day, "Design and control of hybrid magnetic bearings for maglev axial flow blood pump," *2010 IEEE/ASME Int. Conf. Adv. Intell. Mechatronics*, pp. 187–192, Jul. 2010.

[8] C. Sortore, P. Allaire, and E. Maslen, "Permanent magnet biased magnetic bearings, design, construction and testing," *Second Int. Symp. Magn. Bear.*, 1990.

[9] Y. Fan, A. Lee, and F. Hsiao, "Design of a permanent/electromagnetic magnetic bearing-controlled rotor system," *J. Franklin Inst.*, vol. 334, no. 3, 1997.

[10] S. Fukata and K. Yutani, "Dynamics of Permanent-Magnet Biased Active Magnetic Bearings," *Kyushu Univ, Third Int. Symp. Magn. Suspens. Technol.*, pp. 721–736, 1996.

[11] A.-C. Lee, F.-Z. Hsiao, and D. Ko, "Analysis and Testing of Magnetic Bearing with Permanent Magnets for Bias," *JSME Int. journal. Ser. C, Dyn. Control. Robot. Des. Manuf.*, vol. 37, no. 4, pp. 774–782, 1994.

[12] Y. Zhilichev, "Analysis of a magnetic bearing pair with a permanent magnet excitation," *Magn. IEEE Trans.*, vol. 36, no. 5, pp. 3690–3692, 2000.

[13] M. S. Kandil, M. R. Dubois, J. P. Trovão, and and L. S. Bakay, "A Sliding Mode Control of a Hybrid Magnetic Bearing for Wayside Flywheel Energy Storage Systems," in *Vehicle Power and Propulsion Conference (VPPC), 2015 IEEE*, 2015.

[14] A. Hughes, *Electric Motors and Drives: Fundamentals, Types and Applications*. Newnes, 2005.

[15] M. Santina and A. Stubberud, "Discrete-Time Equivalents of Continuous-Time Systems," in *The Control Handbook, Second Edition*, CRC Press, 2010, pp. 12–34.